Role of Transition Metal Catalysts in Single-Walled Carbon Nanotube Growth in Chemical Vapor Deposition

Yoshikazu Homma,* Yoshiro Kobayashi, and Toshio Ogino†

NTT Basic Research Laboratories, Nippon Telegraph and Telephone Corporation, Atsugi 243-0198, Japan

Daisuke Takagi and Roichi Ito

Department of Physics, Meiji University, Tamaku, Kawasaki 214-8571, Japan

Yung Joon Jung and Pulickel M. Ajayan

Department of Materials Science and Engineering, Rensselaer Polytechnic Institute, Troy, New York 12180-3590

Received: May 19, 2003; In Final Form: August 26, 2003

We characterize the iron and cobalt catalysts for carbon nanotube growth in chemical vapor deposition (CVD) by using electron microscopy. Nanoparticles of iron and cobalt exhibit a melting point drop in the methane ambient. Nanoparticles after nanotube growth are identified as Fe_3C and Co_3C for iron and cobalt, respectively. Those results indicate that a eutectic compound of metal and carbon is formed in the methane ambient, resulting in the phase separation into graphite (nanotubes) and metal carbide as the carbon uptake in the catalyst melt increases. This supports the vapor−liquid−solid mechanism for nanotube growth by CVD. Iron or cobalt silicide formation causes the poisoning of the catalysts. However, the coexistence of oxygen due to native oxide on the silicon surface or the metal surface causes formation of a SiO_2 base, which can prevent silicidation of iron particles.

1. Introduction

Carbon nanotubes are self-organized nanoscale structures, and they are expected to have a variety of applications because of their excellent mechanical, electrical, and chemical properties.[1] There are several methods of synthesizing carbon nanotubes, including arc discharge,[2] laser ablation,[3] and chemical vapor deposition (CVD).[4] Among them, CVD is suitable for the carbon-nanotube synthesis on substrates. For electronics applications, site-selective growth of carbon nanotubes is desirable for the integration of nanotube devices on the substrate. In CVD, the nanotube growth temperature is lower than that in other methods, but catalysts are necessary. Single-walled nanotubes (SWNTs) can be selectively grown by CVD by choosing the appropriate combination of carbon-source gas, catalyst, and growth temperature. A variety of combinations has been reported, and typical examples are methane with Fe_2O_3 or CoO at 900−1000 °C,[5] methane with Fe at 900 °C or Co at 800 °C,[6] and alcohol with a mixture of Fe and Co in zeolite powders at 700−800 °C.[7] A comprehensive list of references can be found in ref 7. Iron-family transition metals are mainly used as catalysts. However, the role of the catalyst is still not fully understood. Possible processes are that carbon-bearing molecules are catalytically decomposed on the catalyst surface, resulting in incorporation of carbon atoms into the catalyst. Then once supersaturation occurs, carbon atoms precipitate from the catalyst, leading to nanotube growth. Among these processes, the mechanisms of carbon uptake and supersaturation are not known. The vapor−liquid−solid (VLS) mechanism is one of the proposed explanations.[8,9] This is likely for molten catalyst at high temperature followed by nanotube precipitation during the cooling process in arc discharge and laser ablation. In CVD, however, the temperature is far lower than the melting point of catalyst metals and kept constant during growth. Although catalyst particles often show a molten morphology after the CVD process,[8,10] the exact reason for melting at such low temperatures is not known. Of course, the surface-to-volume ratio in a nanosize particle can affect the melting point.[8] However, nanotubes can grow even from 100-nm-scale particles.[10] Some papers still suppose carbon−metal solid solution for nanotube growth in CVD.[11]

In this paper, we focus on the characterization of iron and cobalt catalysts in methane CVD. We selected a rather simple system consisting of metal catalysts and silicon substrate. We show evidence of eutectic compound formation of metals with carbon. The reaction of these metals with the silicon substrate is also discussed.

2. Experimental Section

For Fe and Co catalysts, commercially obtained nanoparticles and vacuum-deposited thin films were used. Nanoparticles were Fe and Co with a mean particle size of 30 nm and Fe_2O_3 with a mean size of 10 nm (ULVAC Vacuum Metallurgical Co. Ltd.). Si(001) substrates were chemically oxidized in H_2O_2/H_2SO_4 (1:4) solution and dipped in ethanol containing the nanoparticles. An ultrasonic bath was used to uniformly disperse the catalyst particles in the ethanol. Then, the Si substrate with the adsorbed nanoparticles was rinsed in running deionized water to remove large agglomerates of particles. For the thin-film catalyst

* To whom correspondence should be addressed. E-mail: homma@will.brl.ntt.co.jp.

† Present address: Department of Electrical and Computer Engineering, Yokohama National University, Hodogayaku, Yokohama 240-8501, Japan.

10.1021/jp0353845 CCC: $25.00
Published on Web 10/10/2003

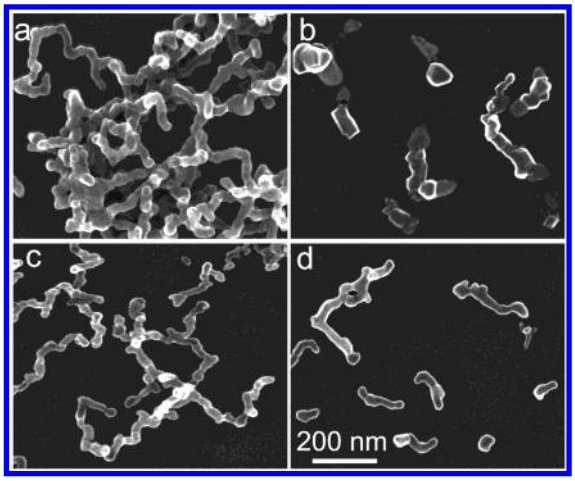

Figure 1. SEM images of Fe nanoparicles with 30-nm diameter (a) after annealing at 850 °C in Ar, (b) after annealing at 900 °C in Ar, (c) after annealing at 600 °C in CH_4, and (d) after annealing at 650 °C in CH_4.

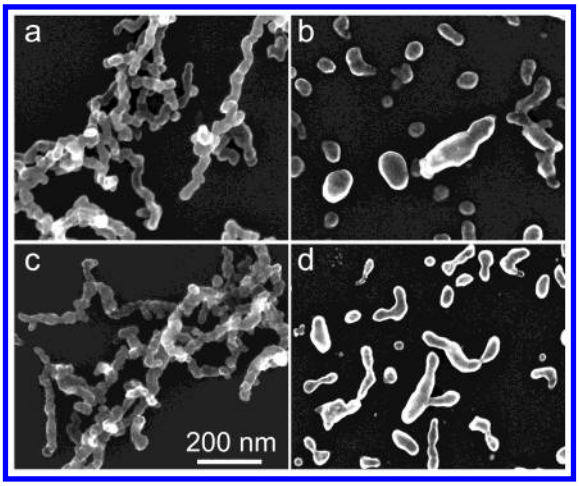

Figure 2. SEM images of Co nanoparicles with 30-nm diameter (a) after annealing at 600 °C in Ar, (b) after annealing at 650 °C in Ar, (c) after annealing at 500 °C in CH_4, and (d) after annealing at 600 °C in CH_4.

preparation, Fe or Co thin film was deposited on the chemically oxidized Si substrate using a conventional vacuum evaporator. The thickness of the deposited film was 0.5 or 5 nm. The deposited film becomes particles during the thermal treatment in CVD growth. The only difference between the nanoparticle and thin films is particle size. The particle size depends on the film thickness. The iron particles were about 8 and 70 nm for the 0.5-nm and 5-nm film, respectively. The cobalt particles were about 6 and 30 nm for these film thicknesses.

The furnace for CVD experiments consisted of a quartz tube and a carbon heater mounted inside a stainless steel chamber. The specimen (10×10 mm^2 or smaller) was placed on a carbon plate (80-mm diameter) above the heater. Argon gas flowed as the furnace was heated to growth temperature (700−950 °C). The argon-gas flow was then replaced by pure methane at a flow rate of 300 cm^3/min with the pressure of 67 kPa. Methane flowed for 1 min and then was replaced by argon to cool the furnace to room temperature. After growth, specimens were observed with a high-resolution scanning electron microscope (SEM, Hitachi S-5000) and a transmission electron microscope (TEM, Hitachi H-9000).

3. Results and Discussion

For methane, SWNTs were selectively obtained on a Si substrate using Fe or Co catalysts, but the optimum conditions were different between the two catalysts. For Fe, the temperature range for SWNT growth depended on particle size. When particle size is 30−100 nm, SWNTs grow at 950−900 °C and multiwalled nanotubes (MWNTs) grow at around 800 °C.[10] The SWNT growth temperature was lowered for smaller Fe particles. SWNTs were obtained at 750−800 °C for ≤10 nm particles. Fe_2O_3 nanoparticles are reduced to Fe during CVD, so the function of Fe_2O_3 is the same as that of the Fe catalyst.[10] However, the particle diameter is different between them because Fe_2O_3 nanoparticles do not agglomerate, while Fe nanoparicles tend to form clusters.[10] For the Co catalyst, on the other hand, the particle size was not critical for the SWNT growth. SWNTs were obtained at around 800 °C. At a higher temperature, no nanotubes were obtained for Co on silicon.

The morphology of Fe nanoparticles observed by SEM is shown in Figure 1 for various temperatures. Before thermal treatment, the iron nanoparticles agglomerated, forming a tree-branch-like structure. In the argon ambient, those particles started to melt at around 900 °C. The reduction of the melting point is due to the nanometer size of the particles. In the methane ambient, the melting point further reduced to 650 °C. A melting point drop was also found for Co nanoparticles (Figure 2). The measured melting points are summarized in Table 1 for Fe and Co within the accuracy of 50 °C. The melting point decreased with decreasing particle size. The melting point in the methane ambient dropped by about 100−200 °C for Fe and about 50 °C for Co compared to that in the argon ambient. The melting point drop for the methane ambient is evidence of the formation of a eutectic compound with carbon. Fe and Co have a phase diagram of a eutectic compound with carbon.[12] The eutectic point of bulk material is 390° and 174° lower than the melting point of Fe and Co, respectively.

TABLE 1: Melting Point of Iron and Cobalt Nanoparticles

	Fe_2O_3 nanopart	Fe nanopart	Fe bulk	Co nanopart	Co bulk
size (nm)	5−10	30		30	
melting point in Ar (°C)	700	900	(1535)	650	(1495)
melting point in CH_4 (°C)	600	650	(1148)[a]	600	(1321)[a]

[a] Eutectic point of Fe−C system.

The melting point of thin films can be evaluated as the temperature at which a continuous film changes to three-dimensional particles, and the resulting particle size can be compared with the nanoparticle cases. The particle size for the 0.5-nm Fe film was 8 nm, and the melting points were the same as those of the 10-nm Fe_2O_3 nanoparticles. The particle size for the 5-nm Fe film was about 70 nm, and the melting points were 1000 and 700 °C in argon and methane, respectively. For the Co film, however, because of the film morphology change at low temperature (<400 °C), it was difficult to determine the melting point.

In the SEM image, the Fe or Fe_2O_3 particles after annealing exhibit a peculiar structure. A central small particle is surrounded by a substance of weaker contrast.[10] Cross-sectional TEM images of nanoparticles are shown in Figure 3, together with electron diffraction patterns. A crystalline particle sits on or beside an amorphous substance. From the electron diffraction pattern, the crystalline particle was identified as orthorhombic Fe_3C (Table 2). Some particles were identified as γ-Fe. On the other hand, compositional data was needed to identify the

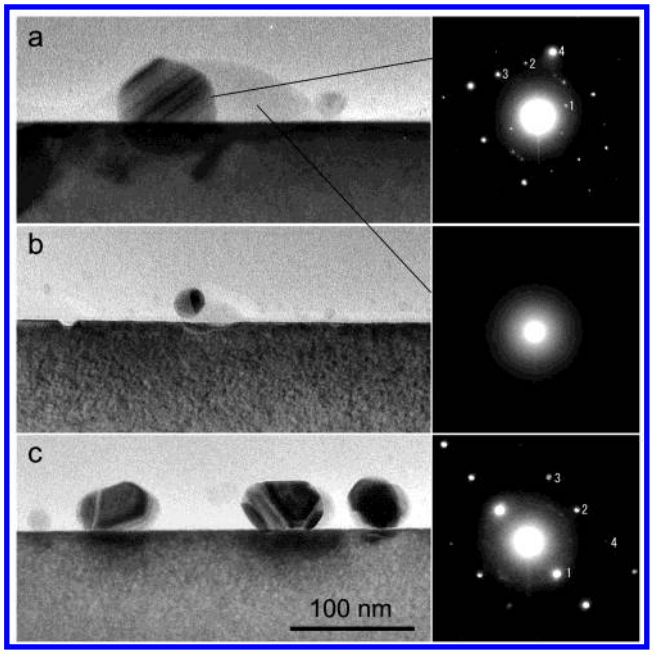

Figure 3. Cross-sectional TEM images and diffraction patterns of nanoparticles after SWNT growth using CH_4: (a) Fe nanoparticles at 950 °C; (b) Fe_2O_3 nanoparticles at 950 °C; (c) Co nanoparticles at 800 °C.

TABLE 2: Analysis of Diffraction Spots from Iron and Cobalt Nanoparticles after CNT Growth

	Figure 3a		Figure 3c	
spot no.	measured d[a] (nm)	Fe_3C d (nm)[b]	measured d (nm)	Co_3C d (nm)[c]
1	0.306	(111) 0.302	0.211	(120) 0.218
2	0.163	(−212) 0.164	0.151	(131) 0.152
3	0.154	(−301) 0.158	0.131	(124) 0.133
4	0.134	(−123) 0.133	0.116	(025) 0.118

[a] d represents interplanar spacing. [b] International Center for Diffraction Data (ICDD) Card 35-772. [c] ICDD Card 26-0450.

amorphous substance. Energy-dispersive X-ray (EDX) spectroscopy indicated that the substance contained silicon and oxygen. Considering that it is amorphous, the substance should be SiO_2. The free-energy difference between SiO_2 and Fe_2O_3 might contribute to the favorable reduction of oxide around the iron-bearing particles and the formation of SiO_2. Thus, SiO_2 is formed selectively around Fe or Fe_2O_3 particles. Strangely, no difference was seen between Fe and Fe_2O_3 nanoparticles in terms of SiO_2 formation. Oxygen might be supplied both from oxide on the particle surface and from that on the substrate surface. The SiO_2 base is thought to prevent reactions between iron particles and the silicon substrate. For Co after 800 °C growth in methane ambient, such SiO_2 formation did not occur (Figure 3c). The particles were identified as orthorhombic Co_3C (Table 2).

When the substrate temperature was high, the reaction between catalyst particles and the substrate occurred (Figure 4). For Fe particles, tetragonal $FeSi_2$ was found above 950 °C (Table 3). In the diffraction pattern, the tetragonal diffraction spots from $FeSi_2$ are superimposed on the Si diffraction spots. Co forms reactants above 850 °C. The reactants showed clear (111) facets and were composed of Si and Co, according to the EDX analysis. The diffraction pattern is attributed to cubic $CoSi_2$ but is quite similar to that of a Si crystal. This may be due to epitaxial formation of $CoSi_2$ because the $CoSi_2$ crystal is cubic and the lattice constant is similar to that of a Si crystal.

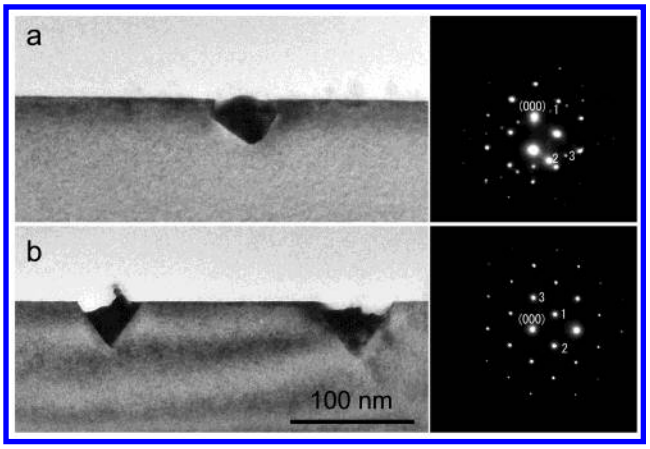

Figure 4. Cross-sectional TEM images and diffraction patterns of nanoparticles after heating at high temperatures in CH_4: (a) Fe nanoparticles at 1000 °C; (b) Co nanoparticles at 950 °C.

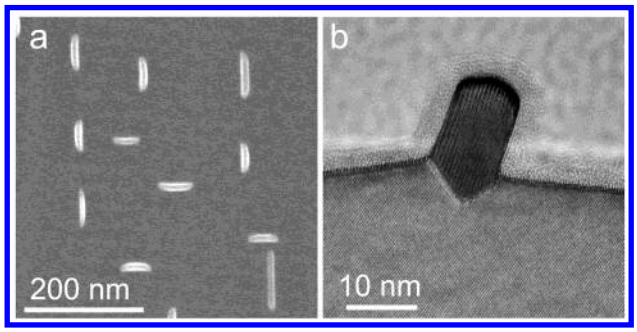

Figure 5. SEM (a) and cross-sectional TEM (b) images of Fe-deposited Si substrate in ultrahigh vacuum. These images were taken after methane CVD at 900 °C.

TABLE 3: Analysis of Diffraction Spots from Iron and Cobalt Nanoparticles after Heating at High Temperatures

	Figure 4a		Figure 4b	
spot no.	measured d (nm)	$FeSi_2$ d (nm)[a]	measured d (nm)	$CoSi_2$ d (nm)[b]
1	0.499	(001) 0.514	0.312	(111) 0.310
2	0.187	(110) 0.190	0.313	(111) 0.310
3	0.181	(111) 0.179	0.267	(200) 0.268

[a] ICDD Card 35-822. [b] ICDD Card 35-1449.

At the silicide-formation temperatures, nanotubes rarely formed for either Fe or Co catalysts. This could have been due to the effects of either silicidation or temperature. Here, we examined solely the effect of silicidation by preparing iron silicide. Iron silicide was grown by Fe deposition in ultrahigh vacuum to avoid SiO_2 formation. The Si(100) substrate was flash-cleaned and deposited with Fe in 2×10^{-6} Pa at the substrate temperature of about 500 °C. Then, the substrate was heated to 800 °C to form silicide and taken out to air. Nanotube growth was performed using methane at 800 or 900 °C. Figure 5 shows an SEM image and a cross-sectional TEM image of the specimen after CVD growth at 900 °C. The silicide crystals have elongated shapes along the ⟨110⟩ directions and have facets along the {111} planes in the substrate. The electron diffraction pattern indicates that the crystals are $FeSi_2$, which is the same as the Figure 4a case. No nanotubes were found for these iron silicide crystals. For the CVD-grown specimen at 800 °C, which is the temperature for multiwalled nanotube growth, nanotube growth was not observed either. These results confirm that nanotubes do not grow from $FeSi_2$. It should be noted that the morphology of the $FeSi_2$ crystals did not changed after CVD growth at 900 °C. This means that the $FeSi_2$ crystals did not

melt in the CVD growth ambient (the melting point of bulk $FeSi_2$ is 1220 °C).[12] Thus, the solidification of silicide might be the reason for the poisoning of the Fe catalyst.

The present study indicates that a carbon−metal liquid is formed during CVD growth. This is due to eutectic compound formation, and an increase in carbon content in the liquid phase causes the phase separation between graphite and the metal. This explains why the transition metals act as catalysts for nanotube growth. Fe, Co, and Ni have a phase diagram in a eutectic compound with carbon, and the eutectic points are 1148, 1321, and 1327 °C, respectively.[12] Because of the size effect, the eutectic point is reduced to 700−800 °C for nanosize particles.

Nanotubes thus grow through the vapor−liquid−solid (VLS) mechanism in CVD. In this respect, the role of the metal particles is not catalytic as in a normal chemical reaction. However, there are three stages in the nanotube formation process: (i) decomposition of hydrocarbon molecules, (ii) carbon incorporation into and precipitation out of the metal particle, and (iii) formation of a graphite structure. The VLS mechanism is related to step ii. The transition-metal particles act as a catalyst in step i. Step iii might also require the catalytic function of the transient metals.

In our experiments, the growth time was short, 1 min. A longer growth time did not increase the SWNT yield. In TEM images, we often find catalyst particles surrounded by graphite layers. These particles may not produce SWNTs any more because methane supply should be hindered by the graphite layers. Graphite layer formation might be a competitive process of SWNT growth. Thus, the SWNT growth may occur in the initial stage of methane supply.

Another type of catalyst poisoning results from the reaction of catalysts with the substrate material. On a Si surface, silicide formation poisons Fe and Co catalysts. SiO_2 formation around an Fe particle can prevent Fe from silicidation. However, if an Fe particle is not fully isolated from the Si substrate by SiO_2 and partially touches the substrate, silicidation can occur. This might be the reason for the lower SWNT yield on Si compared to that on SiO_2 substrate.[13] On the SiO_2 surface, Fe particles do not form silicide below 1000 °C, but they are often embedded under the surface. Even so, the SWNT yield is rather high on the SiO_2 surface. This is a curious phenomenon and should be investigated further.

Zhang et al. selectively grew aligned multiwalled nanotubes on SiO_2 patterns with no growth on Si substrate by simultaneously supplying xylene and vaporized ferrocene.[14] There was no nanotube growth on the bare Si surface due to silicidation of Fe decomposed from ferrocene.[15] The major difference from our case is the absence of native oxide on the Fe particle or on the Si surface. When oxygen and Fe coexist on the Si surface, SiO_2 can be formed between the Fe particle and the Si substrate.

4. Conclusions

We have examined iron and cobalt catalyst morphologies after methane CVD in comparison with those after argon annealing by scanning electron microscopy and found a significant melting point drop in the methane CVD. Transmission electron microscopy in combination with electron diffraction showed Fe_3C or Co_3C formation after CVD. These findings are evidence for eutectic compound formation in the methane ambient. Thus, the growth is mediated by the vapor−liquid−solid mechanism with molten catalysts. Silicidation causes solidification of catalyst particles and thus results in poisoning.

Acknowledgment. We thank Hiroko Sugiyama, Takayuki Kitada, and Seiichiro Mizuno, NTT Advanced Technology Corporation, for TEM and electron diffraction measurements and analyses. This work was carried out with assistance from the NEDO International Joint Research Grant Program.

References and Notes

(1) Dresselhaus, M. S.; Dresselhaus, G.; Avouris, Ph. *Carbon Nanotubes Synthesis, Structures, and Applications*; Springer: Berlin, New York, 2001.

(2) Bethune, D. S.; Kiang, C. H.; deVries, M. S.; Gorman, G.; Savoy, R.; Vazquez, J.; Beyers, R. *Nature* **1993**, *363*, 605.

(3) Thess, A.; Lee, R.; Nikolaev, P.; Dai, H. J.; Petit, P.; Robert, J.; Xu, C. H.; Lee, Y. H.; Kim, S. G.; Rinzler, A. G.; Colbert, D. T.; Scuseria, G. E.; Tomanek, D.; Fischer, J. E.; Smalley, R. E. *Science* **1996**, *273*, 483.

(4) Endo, M.; Takeuchi, K.; Igarashi, S.; Kobori, K.; Shiraishi, M.; Kroto, H. W. *J. Phys. Chem. Solids* **1993**, *54*, 1841.

(5) Kong, J.; Cassell, A. M.; Dai, H. *Chem. Phys. Lett*. **1998**, *292*, 567.

(6) Homma, Y.; Kobayashi, Y.; Ogino, T.; Yamashita. T. *Appl. Phys. Lett*. **2002**, *81*, 2261.

(7) Maruyama, S.; Kojima, R.; Miyauchi, Y.; Chiashi, S.; Kohno, M. *Chem. Phys. Lett.* **2002**, *360*, 229.

(8) Kukovitsky, E. F.; L'vov, S. G.; Sainov, N. A. *Chem. Phys. Lett*. **2000**, *317*, 65.

(9) Gavillet, J.; Loiseau, A.; Journet, C.; Willaime, F.; Ducastelle, F.; Charlier, J.-C. *Phys. Rev. Lett*. **2001**, *87*, 275504.

(10) Homma, Y.; Yamashita, T.; Finnie, P.; Tomita, M.; Ogino, T. *Jpn. J. Appl. Phys*., *Part 2* **2002**, *41*, L89.

(11) Li, Y.; Kim, W.; Zhag, Y.; Rolandi, M.; Wang, D.; Dai, H. *J. Phys. Chem. B* **2001**, *105*, 11424.

(12) Massalski, T. B.; Murray, J. L.; Bennett, L. H.; Baker, H.; Kacprzak, L. *Binary Alloy Phase Diagrams*; American Society for Metals: Metals Park, OH, 1986; Vols. 1 and 2.

(13) Jung, Y. J, Homma, Y.; Ogino, T.; Kobayashi, Y.; Takagi, D.; Wei, B. Q.; Vajtai, R.; Ajayan, P. M. *J. Phys. Chem. B* **2003**, *107*, 6859.

(14) Zhang, Z. J.; Wei, B. Q.; Ramanath, G.; Ajayan, P. M. *Appl. Phys. Lett*. **2000**, *77*, 3764.

(15) Jung, Y. J.; Wei, B. Q.; Vajtai, R.; Ajayan, P. M.; Homma, Y.; Prabhakaran, K.; Ogino, T. *Nano Lett*. **2003**, *3*, 561.